Mitochondrial Function in Oxidative and Glycolytic Bovine Skeletal Muscle Postmortem

Patricia M. Ramos[1], Lindsey C. Bell[1], Stephanie E. Wohlgemuth[2], and Tracy L. Scheffler[1]*

[1]Department of Animal Sciences, University of Florida, Gainesville, FL 32611, USA
[2]Department of Aging and Geriatric Research, University of Florida, Gainesville, FL 32603, USA
*Corresponding author. Email: tscheffler@ufl.edu (Tracy L. Scheffler)

Abstract: Meat quality is traditionally associated with anaerobic metabolism due to cessation of the oxygen supply postmortem. However, mitochondrial (mt) function early postmortem may affect the development of meat quality characteristics, such as adenosine triphosphate levels and pH decline. Therefore, the objective of this study was to evaluate mt function *ex vivo* during the first 24 h postmortem in muscles with differences in mt content. Samples from *longissimus lumborum* (LL) and *diaphragm* (Dia) were taken from steers ($n = 6$) at 1, 3, and 24 h postmortem and frozen to determine citrate synthase (CS) activity and mt protein expression (immunodetection) or were fresh-preserved for high-resolution respirometry. Integrative oxygen consumption rate (picomoles per second per milligram of tissue) was measured and normalized to CS activity as a proxy for mt content (intrinsic mt function, picomoles per second per unit CS). CS activity ($P < 0.001$) and mt protein expression ($P < 0.001$) were greater in Dia, which was reflected in mt respiration. Muscle type affected ($P < 0.001$) integrative leak respiration and was greater in mt from Dia; oxidative phosphorylation (OXPHOS) was also greater in Dia and influenced by time postmortem (muscle × time: $P = 0.01$). Intrinsic leak and OXPHOS were affected by muscle and time (muscle × time: $P = 0.05$ and $P = 0.01$, respectively), with the most pronounced differences at 24 h postmortem. Stimulation of OXPHOS by cytochrome *c* as an indicator of outer mt membrane integrity was influenced by muscle and time postmortem (muscle × time: $P = 0.03$); it was greater in mt from LL. Despite intrinsic differences in respiratory function at 24 h, mt from both muscles were intact and coupled at 1 h postmortem. Reduced content and respiratory function in mt from LL are associated with early fragmentation, which could impact protease activation and subsequently meat quality.

Introduction

At slaughter, exsanguination eliminates the blood supply to the muscle, limiting oxygen for aerobic metabolism. Consequently, mitochondrial (mt; note: the abbreviation "mt" is subsequently used for "mitochondrial" and "mitochondria") contributions to postmortem metabolism and meat quality development are often disregarded. However, there is a strong possibility that mt affect the energetic and biochemical milieu in muscle early postmortem. In addition to their role in energy production, mt influence calcium dynamics, oxidative stress, and apoptosis signaling (Powers et al., 2011; Williams et al., 2013). These functions could have profound implications for fundamental aspects of meat quality development, such as pH decline and proteolysis.

Mt function and integrity are highly dependent on the mt membrane potential, which refers to the uneven charge distribution between the mt intermembrane space and the mt matrix. Under normal physiological conditions, adenosine triphosphate (ATP) synthesis is powered by the flow of protons to the matrix through the F_o subunit of the F_oF_1 ATPase (also referred to as complex V). Conditions such as hypoxia and oxidative stress impair mt ATP

production and can be disastrous for mt structure and function. An imbalance in ATP demand and production results in elevated sarcoplasmic calcium, causing mt to accumulate significant amounts of calcium (Kwong and Molkentin, 2015). Mt calcium overload induces opening of a pore in the inner mt membrane (mt permeability transition pore) (Halestrap, 2009), which causes collapse of the mt membrane potential, reverse operation of the F_oF_1 ATPase (ATP hydrolysis), and release of calcium from the mt. Ions and small molecules enter the mt matrix, culminating in mt swelling and outer mt membrane permeabilization, followed by release of cytochrome *c* (cyt *c*) and other proapoptotic proteins from the mt matrix or intermembrane space into the cytosol. Apoptotic and necrotic cell death are the ultimate consequence of these events. While cyt *c* release and ATP are requisite for activation and cleavage of caspases in apoptosis (Liu et al., 1996), outer membrane permeabilization and cyt *c* release to the cytosol may also occur in necrosis or caspase-independent cell death, and crosstalk between pathways exists (Tait and Green, 2010; Karch and Molkentin, 2015; Bock and Tait, 2020). Sarcoplasmic calcium fluctuations, ATP depletion, and proteolysis throughout this process are likely affecting meat quality development. For example, calcium overload and necrosis directly implicate calpains, which are well-established to contribute to postmortem proteolysis, and apoptosis has been proposed to influence tenderization by caspase-mediated cleavage of calpastatin, thereby increasing calpain activity.

Yet changes in mt structure and function early postmortem are poorly understood. Mt isolated from postmortem muscle within the first hour after exsanguination can respire and are well coupled (England et al., 2018). The decline in mt function with time postmortem is associated with rate of pH decline. For example, isolated mt from the *triceps* of dark-cutting beef (ultimate pH of 6.6–6.7) are reasonably well coupled at 5 d postmortem compared with mt isolated from control beef with ultimate pH of 5.6–5.7 (Ashmore et al., 1972). Respiratory activity in permeabilized fibers declines to a greater extent in *longissimus* from malignant hyperthermia-positive pigs compared with genotypes with slower pH decline (Werner et al., 2010). On the other hand, Tang et al. (2005) observed a rapid decline in pH in bovine cardiac muscle (pH ~ 6.0 at 30 min postmortem), but mt isolated from bovine heart 2 h postmortem still exhibited adenosine diphosphate (ADP)-stimulated respiration and were relatively well coupled. Thus, the relationship between pH decline and mt function postmortem may depend on the contractile

and metabolic properties and mt content of muscle fibers.

Understanding changes in mt function postmortem is further complicated by distinct mt populations within fibers. Not only does mt content vary among fiber types, but unique populations of mt exist within a muscle fiber. Subsarcolemmal mt are located at the fiber's periphery, beneath the sarcolemma, and intermyofibrillar mt are positioned between the myofibrils. These mt populations display different functions and susceptibility to mt permeability transition (Adhihetty et al., 2005; Sollanek et al., 2017). Mt exhibit distinct phenotypes and form dynamic networks to meet the contractile demands of the muscle. Comparison of intermyofibrillar mt in glycolytic, oxidative, and cardiac muscles revealed that the mt network configuration, shape and size, and the junctions connecting mt are optimized for either calcium uptake or energy distribution functions (Bleck et al., 2018). These functions are also related to physical associations between mt and other cellular components, including the microtubules of the cytoskeleton, sarcoplasmic reticulum, and lipids (Boncompagni et al., 2009; Varikmaa et al., 2014; Bleck et al., 2018).

Based on the distinct phenotypes and functions of mt, we expect that mt in oxidative and glycolytic muscles exhibit different innate functional properties during the postmortem period. Therefore, our objective was to assess function and outer membrane integrity postmortem of mt from metabolically distinct bovine skeletal muscles with expected differences in mt content. We assessed mt respiratory function *ex vivo* using permeabilized myofibers, which permits assessment of mt within their normal cellular location and environment, and without disrupting associations between mt or their connections to other intracellular components. We hypothesized that *diaphragm* (Dia) would have greater integrative (i.e., per unit mass) mt content and oxidative phosphorylation (OXPHOS) capacity compared with *longissimus lumborum* (LL) and that mt from the more glycolytic LL would exhibit a greater functional decline 24 h postmortem.

Materials and Methods

Animals and sampling

Steers ($n = 6$) of primarily Angus (80%–100% Angus; 0%–20% Brahman) genetics were harvested at approximately 18.5 mo and 630 kg live weight at the University of Florida Meat Processing Center, under inspection by the United States Department of

Agriculture Food Safety and Inspection Service. The slaughters were on 3 different days during the summer (2 animals per day), and samples from the LL and the Dia were collected at 1, 3, and 24 h postmortem. Carcass sides were placed in the cooler at approximately 1.25 h postmortem. Samples from the LL were collected from the left carcass side: the 1-h sample was taken ~10 cm posterior to the last rib, the 3-h sample was collected near the last rib, and the 24-h sample was collected from ~10 cm posterior to the initial sample site. For the Dia, the 1-h sample was taken from the left carcass side ~15 cm distal to the midline, and the 3-h sample was collected ~15 cm distal to the initial site. The 24-h sample from the Dia was collected from the right side at a similar position as the 1-h site.

Muscle samples were designated for immediate analysis (respirometry) or frozen in liquid nitrogen and stored at −80°C until analysis. The pH of each muscle was obtained using a pH meter (HI99163, Hanna Instruments, Woonsocket, RI) at the same time as sampling, as well as muscle temperature.

High-resolution respirometry

Samples were immediately cleaned from adipose tissue and connective tissue and immersed in ice-cold biopsy preservation buffer (BIOPS; 2.77 mM CaK$_2$ethylene glycol-bis(β-aminoethyl ether)-N,N,N, N'-tetracetic acid [EGTA], 7.23 mM K$_2$EGTA, 5.77 mM Na$_2$ATP, 6.56 mM MgCl$_2$·6H$_2$O, 20 mM taurine, 15 mM Na$_2$Phosphocreatine, 20 mM imidazole, 0.5 mM dithiothreitol and 50 mM 2-(N-morpholino)ethanesulfonic acid, pH adjusted at 0°C to 7.1 using 5 N KOH; Eigentler et al., 2012). Using a dissection microscope, fresh-muscle bundles immersed in ice-cold BIOPS were finely cleaned, and fibers were teased using a pair of forceps (Kuznetsov et al., 2008). Bundles were transferred to a 12-well plate that contained ice-cold permeabilization solution (50 μg saponin/mL BIOPS). Bundles were permeabilized for 10 min at 4°C on a rotator, and then washed for 10 min in mt respiration medium (MiR05; 0.5 mM EGTA, 3 mM MgCl$_2$·6H$_2$O, 60 mM lactobionic acid, 20 mM taurine, 10 mM KH$_2$PO4, 20 mM 4-(2-hydroxyethyl)piperazine-1-ethanesulfonic acid, 110 mM D-sucrose and 1 g/L bovine serum albumin essentially fat acid free, pH 7.1; Fasching et al., 2016). Bundles were gently blotted dry using filter paper, and weight (milligrams) was recorded (2–4 mg tissue). Bundles were immediately transferred to previously calibrated oxygraph chambers maintained at 39°C (Oroboros O2K; Oroboros Instruments, Innsbruck, Austria) containing MiR05.

Mt respiration was determined in duplicate under hyperoxic conditions (290–450 μM O$_2$) as previously described (Li et al., 2016). Oxygen consumption rate (OCR; picomoles per second per milligram of tissue) was determined using the following substrate-

Figure 1. Example trace showing the respirometry protocol with permeabilized muscle fibers from *longissimus lumborum* muscle at 1 h postmortem. Oxygen flux per tissue mass (ρmol/s/mg wet weight tissue; red line) and oxygen concentration (nmol/mL; blue line). The following SUIT protocol was performed: (1) malate, pyruvate (2 and 5 mM, respectively; leak respiration [or L]); (2) ADP (2.5 mM; activated respiration, OXPHOS, P$_{CI(PM)}$); (3) glutamate (10 mM; activated respiration, OXPHOS, P$_{CI(PMG)}$), (4) succinate (10 mM; activated respiration, OXPHOS, P$_{CI+II}$), (4) cytochrome *c* (10 μM; outer mt membrane integrity, cyt *c*, see text for details); (5) FCCP (0.05 μM steps; maximum ETS, E$_{CI+II}$); (8) antimycin A (2.5 μM; ROX). ADP, adenosine diphosphate; cyt *c*, cytochrome *c*; ETS, electron transport system; FCCP, carbonyl cyanide 4-(trifluoromethoxy) phenylhydrazone; mt, mitochondria/mitochondrial; OXPHOS, oxidative phosphorylation; ROX, residual oxygen consumption; SUIT, substrate-uncoupler-inhibitor-titration.

uncoupler-inhibitor-titration protocol (Figure 1; concentration of reagents noted in parentheses are final within chambers): (1) leak (L) respiration was assessed after tricarboxylic acid (TCA) cycle stimulation with nicotinamide-adenine-dinucleotide-linked substrates pyruvate (5 mM) and malate (2 mM) to support electron flow through complex I (CI) of the electron transport system (ETS) (E); (2) OXPHOS (P) was stimulated with ADP (2.5 mM) and recorded as $P_{CI (PM)}$; (3) glutamate (10 mM) influence on nicotinamide adenine dinucleotide production and respiration (CI) was tested and recorded as $P_{CI(PMG)}$; (4) addition of succinate (10 mM) supported convergent electron flow through complexes I and II of the ETS (OXPHOS; P_{CI+II}); (5) mt outer membrane integrity was tested by cyt c (10 μM) addition; (6) stepwise titration of the uncoupler carbonyl cyanide 4-(trifluoromethoxy) phenylhydrazone (FCCP; 0.5 μL of a 0.1 mM stock solution) was added to reach maximum uncoupled respiration and recorded as maximum ETS capacity (E_{CI+II}); and (8) addition of antimycin A (2.5 μM) inhibited complex III of the ETS and thereby OXPHOS, and the remaining OCR was recorded as residual oxygen consumption (ROX). For the calculation of OCR during the respiratory states (L, P, E), non-mt oxygen consumption, ROX, was subtracted from all preceding states. Complex II (CII) capacity (P_{CII}) was calculated as $P_{CI+II} - P_{CI}$. Maximum OCR (OCR_{max}) represents the greatest OCR achieved during the substrate-uncoupler-inhibitor-titration protocol (corrected for ROX) and occurred either after cyt c or after FCCP addition. Coupling control factors (CCF) for CI and CI + CII were calculated as $1 - (L/P_{CI})$ and $1 - (L/P_{CI+II})$, respectively, and excess capacity factor as $1 - (P_{CI+II}/OCR_{max})$.

Citrate synthase activity

Muscle samples from all animals, muscles, and time points ($n = 36$ total) were powdered in liquid nitrogen, and approximately 50 mg was diluted 1:20 (w/v) in buffer (0.25 M sucrose, 1 mM ethylenedinitrilotetracetic acid, 10 mM Tris-HCl [pH 7.4]), processed, and assayed for citrate synthase (CS) activity in triplicate as previously described by Wright et al. (2018). Activity was calculated using a linear increase interval of 4 min according to the Beer-Lambert equation and expressed as nanomoles per minute per milligram of tissue.

Mitochondrial protein expression

Powdered muscle tissue (approximately 100 mg; $n = 36$ total) was processed to extract mt proteins as described by Wadley and McConell (2007). Briefly, pulverized samples were diluted 1:10 (w/v) with extraction buffer (50 mM Tris-base; 1 mM ethylenedi-nitrilotetracetic acid [pH adjusted at cold to 7.5]; supplemented with 10% glycerol, 1% Triton-X, 50 mM sodium fluoride, 1 mM dithiothreitol, and 5 μL/mL protease inhibitor cocktail [Sigma, St. Louis, MO]) and homogenized once at 5,000 rpm for 10 s with a bead homogenizer (Precellys 24 Homogenizer; Bertin Instruments, Hialeah, FL), followed by sonication (10×1 s) and incubation on ice for 20 min. Supernatant was collected after centrifugation at $10,000 \times g$ for 20 min at 4°C. Protein concentration was determined using a bicinchoninic acid protein assay (Thermo Scientific, Rockford, IL), and supernatants were diluted with extraction buffer and 5× Laemmli buffer (0.5 M tris-base [pH 6.8], 0.5 M dithiothreitol, 10% sodium dodecyl sulfate (SDS), 0.5% bromophenol blue, and 50% glycerol) to achieve equal protein concentrations. Samples were heated at 95°C for 5 min and then stored at −20°C. Proteins were separated by SDS polyacrylamide gel electrophoresis (MGV-202-20, C.B.S. Scientific, San Diego, CA) using 10% polyacrylamide resolving gels (37.5:1 acrylamide: bis-acrylamide; 0.375 M Tris-HCl [pH 8.8]; 0.1% SDS [w/v]; 0.1% [w/v] ammonium persulfate; and 0.001% [v/v] tetramethylethylenediamine) and 5% stacking gels (37.5:1 acrylamide: bis-acrylamide; 0.125 M Tris-HCl [pH 6.8]; 0.1% SDS [w/v]; 0.1% [w/v] ammonium persulfate; and 0.001% [v/v] tetramethylethylenediamine), and wells were loaded with equal amounts of protein (15 μg). Electrophoresis running buffer (25 mM tris-base, 0.2 M glycine, and 0.1% SDS) was used, and run was performed at 60 V for 20 min, followed by 125 V for 1 h 10 min. Proteins were transferred to a nitrocellulose membrane (Thermo Scientific, Rockford, IL) using wet tank transfer (EBU 402, CBS Scientific, San Diego, CA) at 500 mA and 4°C for 1 h with cold transfer buffer (50 mM tris-base, 0.38 M glycine, 0.01% SDS, and 10% methanol). Subsequently, the membrane was dried overnight. Since muscles used have different contractile properties, the protein profile was expected to differ (see Figure 2B). Total protein stain (REVERT, LI-COR, Lincoln, NE) was used to validate equal protein loading and to normalize target protein signal within a lane, with membrane scanned using an Odyssey CLx imager (LI-COR, Lincoln, NE) and quantified using Image Studio software version 5.2 (LI-COR). After total protein staining, the membrane was used for immunodetection of CS and iron-sulfur protein subunit of succinate dehydrogenase (SDHB). Membranes were washed in 1× Tris-buffered

(a)

(b)

(c)

(d)
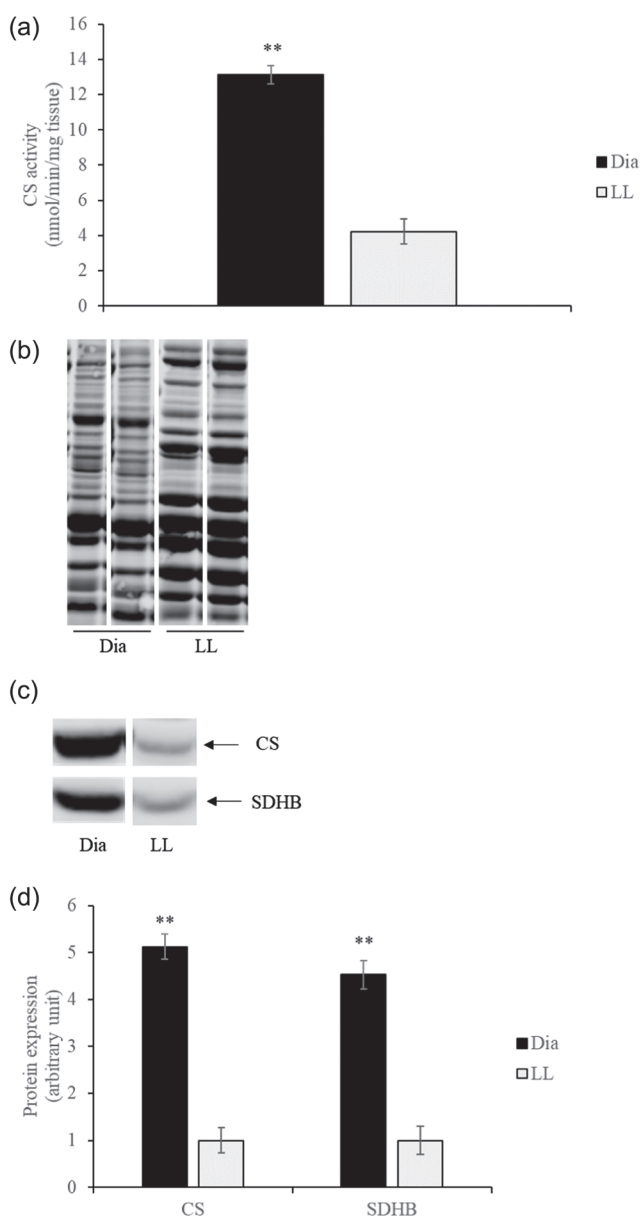
Figure 2. (a) CS activity (nmol/min/mg wet weight tissue), (b) REVERT protein stain of electrophoretically separated proteins, electrotransferred to a nitrocellulose membrane (2 representative lanes per muscle, bovine LL and Dia), (b) representative western blot bands probed for CS and SDHB, respectively, and (d) protein expression from quantification of western blot bands representing mitochondrial CS and iron-sulfur protein subunit of SDHB from bovine LL and Dia, presented as arbitrary units relative to LL. **Muscle: $P < 0.001$. CS, citrate synthase; Dia, *diaphragm*; LL, *longissimus lumborum*; SDHB, succinate dehydrogenase B subunit.

saline (TBS; pH 7.6) for 2 min and then blocked with Starting Block (TBS) Blocking Buffer (Thermo Scientific, Rockford, IL) for 1 h. Primary antibodies for CS and SDHB (ab96600 and ab14714, respectively; Abcam, Cambridge, MA) were diluted 1:1,000 in blocking buffer with 0.2% Tween 20, and membranes were incubated at 4°C overnight with agitation. Membranes were then washed 4 times with 1× TBS

with 0.1% Tween 20 for 5 min and incubated for 1 h in secondary antibody conjugated with fluorescent dye (IRDye 800CW, LI-COR, Lincoln, NE), diluted 1:10,000 in blocking buffer with 0.2% Tween 20. Finally, membranes were washed 4 times with 1× TBS-0.1% Tween 20 for 5 min each, followed by an additional wash with 1× TBS (pH 7.6). Membranes were then scanned, and the signals for the respective target bands were quantified using Image Studio software.

Statistical analysis

Muscle (LL and Dia), time postmortem (1, 3, and 24 h), and their interaction were the fixed effects investigated in a complete randomized block design. Block was slaughter dates, used as random effect in the mixed procedure from SAS software version (SAS Institute Inc., Cary, NC), University Edition. Time was considered a repeated measure. Normal distribution of residuals and homogeneity of variance were tested, and data transformed when needed. When interaction was significant, the slice statement was used to investigate levels within a factor. Differences between least-squares means were separated using the PDIFF option. Effects were considered significant at $P < 0.05$ and tendencies at $P < 0.10$. Results are presented as least-squares means estimate and standard error.

Results and Discussion

Mitochondrial content: Citrate synthase activity and protein expression

Skeletal muscle fibers exhibit functional heterogeneity in order to accomplish a wide variety of tasks. Contractile and metabolic properties range from slow-contracting, oxidative fibers constructed for endurance to fast-contracting, glycolytic fibers designed for short-duration, high-intensity work. Previously, mt content was thought to drive differences in energy metabolism between fiber types, but there is growing evidence that mt may exhibit specific phenotypes based on fiber type properties and location in the cell (Palmer et al., 1977; Schmidt and Herpin, 1998; Hofer et al., 2009). In turn, these mt properties may differentially influence mt function and muscle metabolism during the postmortem period.

We used Dia and LL to represent muscles with distinct metabolic properties and differences in mt content. The Dia, which supports breathing, is a slow, oxidative muscle composed of primarily myosin heavy chain isoform type I (Scheffler et al., 2018). In contrast,

the LL extends the spine and is a fast, glycolytic muscle with a high proportion of type IIa and IIx myosin heavy chain (Muroya et al., 2002; Toniolo et al., 2005; Scheffler et al., 2018). CS activity, a marker of mt content (Larsen et al., 2012), differed between muscles ($P < 0.001$), with Dia exhibiting 3.2-fold greater CS activity compared with LL (Figure 2A). Expression of mt proteins CS and SDHB (Figure 2C–2D) was 5.1 and 4.5 times greater, respectively, in Dia compared with LL muscle ($P < 0.001$), confirming the results obtained with CS activity measurements.

Integrative versus intrinsic mitochondrial function postmortem

In this study, we used a permeabilization protocol for muscle fibers that permits assessment of the entire mt population in situ and preserves mt morphology. In contrast, mt isolation protocols might lead to changes in mt morphology and misrepresentation of mt functional status (Picard et al., 2010). Mt respiratory function of a muscle fiber bundle, or integrative mt function—expressed as OCR per tissue mass (picomoles oxygen per second per milligram of tissue; Figure 3A, Figure 4A and 4C, Figure 5A)—can be driven by the fibers' mt content, and accordingly, variation in mt content related to muscle fiber type composition is expected to contribute to differences in integrative mt function between muscles. To normalize mt respiration to mt content, integrative OCR was divided by CS activity, a proxy measure of mt content. The resulting intrinsic respiratory activity (picomoles oxygen per second per unit CS; Figure 3B, Figure 4B and 4D, Figure 5B) represents mt respiratory function per mt unit.

Leak respiration

We first investigated proton conductance through the inner mt membrane, known as leak respiration. Integrative leak was greater in Dia compared with LL (main effect of muscle: $P < 0.001$; Figure 3A), with no differences over time postmortem ($P = 0.81$) or interaction (muscle × time: $P = 0.39$). At 1 h postmortem, leak in Dia tended ($P = 0.08$) to be greater, and at 3 h and 24 h, leak was significantly greater than in LL ($P = 0.02$ and 24 h $P < 0.001$, respectively; Figure 3A). However, when normalized to mt unit, intrinsic leak tended to be greater in LL compared with Dia (main effect of muscle: $P = 0.09$; and $P = 0.07$ between LL and Dia at 3 h postmortem; Figure 3B). In addition, LL and Dia exhibited different patterns for intrinsic leak with time postmortem (muscle × time: $P = 0.05$). In LL, intrinsic leak tended to decrease
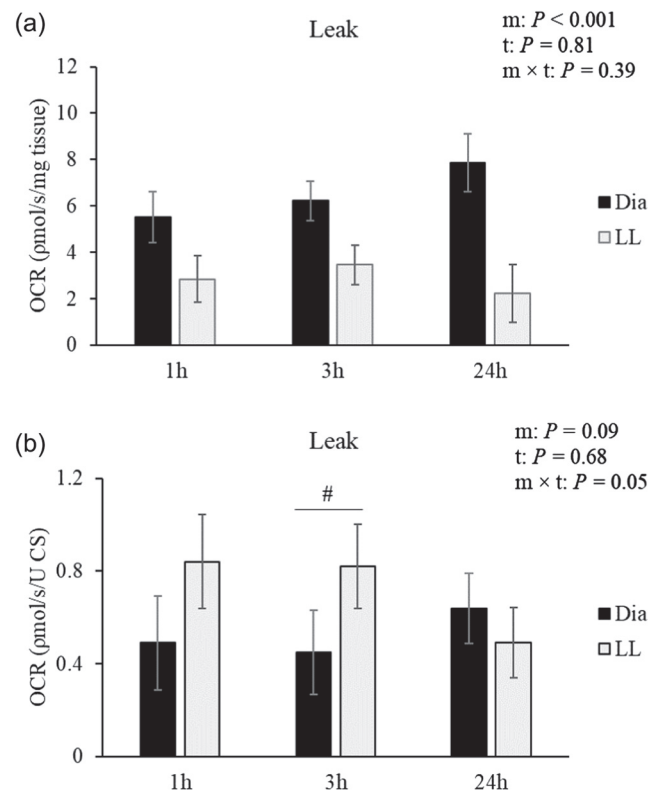
Figure 3. (a) Integrative (ρmol/s/mg wet weight tissue) and (b) intrinsic (ρmol/s/U CS) OCR representing leak respiration stimulated by pyruvate and malate in the absence of ADP in permeabilized muscle fibers from bovine LL and Dia collected at 1, 3, and 24 h postmortem. [a,b]Different letters represent $P < 0.05$. [#]Represents the trend between muscles within 3 h postmortem ($P = 0.07$). ADP, adenosine diphosphate; CS, citrate synthase; Dia, *diaphragm*; LL, *longissimus lumborum*; OCR, oxygen consumption rate. m, main effect of muscle; t, main effect of time; m x t, muscle and time interaction.

over time ($P = 0.07$), with similar rates at 1 h and 3 h but numerically lower values at 24 h. In comparison, time postmortem did not affect leak in Dia ($P = 0.48$).

Oxygen consumption mediated by leak is not coupled to ATP synthesis and represents the proton leak across the inner mt membrane; the relative contribution of leak to total OCR decreases considerably as work intensity increases (Korzeniewski, 2017). The relationship between proton leak and muscle fiber type is not well established, and inconsistent findings (Leary et al., 2003; Glancy and Balaban, 2011; Park et al., 2014) may be partly due to methods for functional assessment of mt (isolated mt vs. permeabilized fibers) and approaches to normalize to mt content. Similar to our findings, in horses, integrative leak in mt of permeabilized fibers from oxidative *triceps brachii* tended to be greater than from more glycolytic *gluteus medius*, but after normalization to CS activity (as a proxy for mt content), intrinsic leak tended to be greater in the
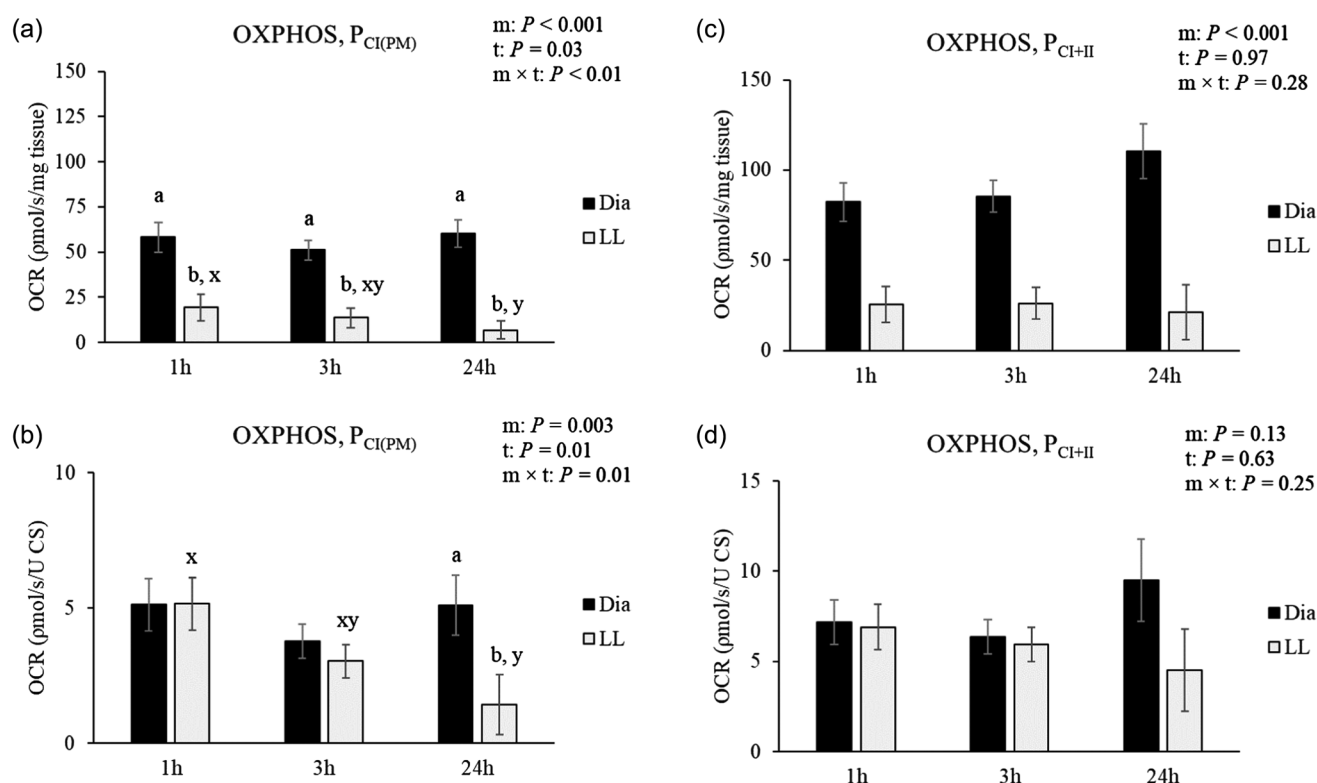
Figure 4. (a) and (c) integrative (ρmol/s/mg wet weight tissue) and (b) and (d) intrinsic (ρmol/s/U CS) OCR representing activated respiration (OXPHOS) when stimulated by pyruvate and malate (a and b) and succinate (c and d) in the presence of ADP in permeabilized muscle fibers from bovine LL and Dia collected at 1, 3, and 24 h postmortem. [a,b]Different letters represent differences between muscles (muscle effect: $P < 0.05$) within time. [x,y]Different letters represent differences between time point (time effect: $P < 0.05$) within muscle. ADP, adenosine diphosphate; CS, citrate synthase; Dia, *diaphragm*; LL, *longissimus lumborum*; OCR, oxygen consumption rate; OXPHOS, oxidative phosphorylation. m, main effect of muscle; t, main effect of time; m x t, muscle and time interaction.

gluteus medius (Li et al., 2016). Increased proton leak per mt in glycolytic fibers may be a means of limiting reactive oxygen species production and limiting oxidative damage (Skulachev, 1996; Brand, 2000). Thus, mt content as well as intrinsic mt or fiber properties may contribute to differences in leak respiration between muscles.

Oxidative phosphorylation

Addition of ADP stimulated respiration with CI supporting substrates (pyruvate and malate; $P_{CI(PM)}$; Figure 4A). At 1 h postmortem, ADP increased OCR (P_{CI}) approximately 10-fold in Dia and 7-fold in LL relative to leak. A similar increase in mt respiration using bovine LL was previously reported (Ramos et al., 2020a); however, glutamate was used in addition to pyruvate and malate. In the present study, we did not observe a further increase upon glutamate addition (0%–6% increase relative to $P_{CI(PM)}$, data not shown). Thus, pyruvate and malate were sufficient to support nearly all CI-driven respiration in the presence of ADP. Integrative OCR was greater in mt from Dia compared with LL at all times

analyzed, which was expected due to greater mt content. Whereas Dia exhibited similar P_{CI} regardless of time, P_{CI} for LL mt decreased during the postmortem period (muscle × time: $P < 0.01$). Interestingly, even at 24 h postmortem, Dia showed similar OCR compared with 1 h (average 56.6 ρmol/s/mg tissue), whereas in LL, values declined almost 3-fold during the same period. When OCR was normalized to CS activity, the contrasting patterns for P_{CI} in LL and Dia over time were preserved ($P_{CI(PM)}$ muscle × time: $P = 0.01$; Figure 4B). The intrinsic OXPHOS capacity with CI-supporting substrates in LL mt decreased from 1 h to 24 h ($P < 0.001$), whereas it remained similar over time in Dia mt. At 1 and 3 h postmortem, mt from Dia and LL exhibited similar intrinsic P_{CI}, supporting that differences in integrative P_{CI} between muscles early postmortem are largely due to mt content. In contrast, greater intrinsic $P_{CI(PM)}$ in Dia compared with LL at 24 h ($P < 0.001$) corroborates that qualitative differences between mt from these muscles are contributing to variation in mt function later postmortem.

Subsequent addition of succinate allowed convergent electron flow through both CI and CII (P_{CI+II}), further enhancing OCR. Compared with P_{CI}, succinate
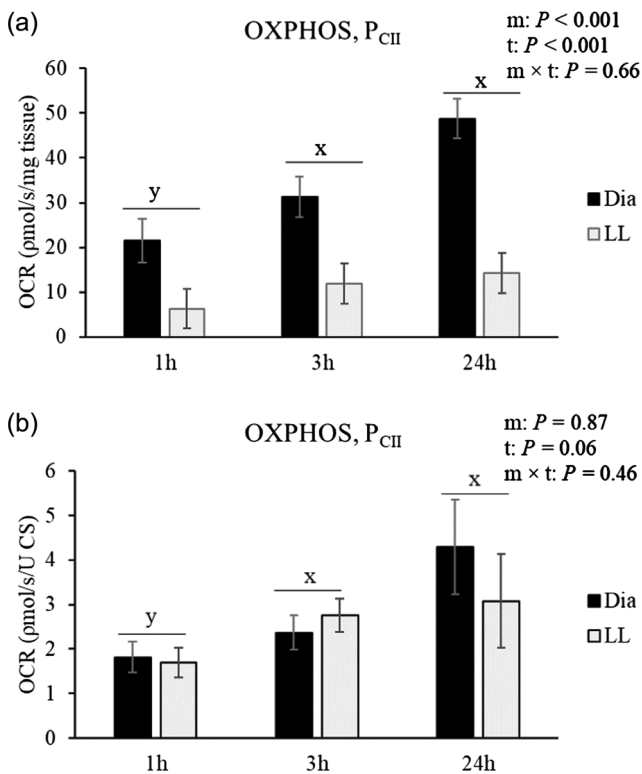
(a)

(b)

Figure 5. (a) Integrative (ρmol/s/mg wet weight tissue) and (b) intrinsic (ρmol/s/U CS) OCR representing activated respiration (OXPHOS) when stimulated by pyruvate, malate, glutamate, and succinate in the presence of ADP in permeabilized muscle fibers from bovine LL and Dia collected at 1, 3, and 24 h postmortem. Data are presented as complex II capacity (P_{CII}), which was calculated as $P_{CI+II} − P_{CI}$. [a–d]Different letters represents differences within muscle and time ($P < 0.05$). [x,y]Different letters represent differences between time point (time effect: $P < 0.05$) considering both muscles. ADP, adenosine diphosphate; CS, citrate synthase; Dia, *diaphragm*; LL, *longissimus lumborum*; OCR, oxygen consumption rate; OXPHOS, oxidative phosphorylation. m, main effect of muscle; t, main effect of time; m x t, muscle and time interaction.

increased OCR approximately 1.3-fold for both muscles at 1 h postmortem (Figure 4C). Similar to P_{CI}, P_{CI+II} was greater in Dia compared with LL regardless of time (main effect of muscle: $P < 0.001$). Intrinsic mt function with CI and CII substrates was similar between muscles postmortem ($P = 0.13$), and there was no effect of time ($P = 0.63$) nor interaction (muscle × time: $P = 0.25$; Figure 4D). Similar to intrinsic $P_{CI(PM)}$, intrinsic OCR for CI+II was similar between muscles at 1 h and 3 h, but by 24 h, respiration of LL mt was numerically less than Dia mt.

Dia displayed consistently greater integrative leak and OXPHOS, which is in agreement with predominantly aerobic energy metabolism and greater mt content of this muscle, confirmed by CS activity and mt protein expression (Figure 2). However, at 1 h postmortem, intrinsic mt OXPHOS capacity was similar between Dia and LL, indicating that early postmortem—and potentially antemortem—mt respiratory

function of the mt unit across all potential mt populations present in the muscle fibers was independent of the muscles' fiber type properties. Consistent with our findings, Park et al. (2014) observed that heart, skeletal, and smooth muscle fibers exhibited large differences in CS activity, but OXPHOS capacity per mt (as per CS activity) was similar. However, in horses, the more glycolytic *gluteus medius* had a lower integrative but a greater intrinsic OXPHOS capacity compared with the more oxidative *triceps* muscle (Li et al., 2016).

The glycolytic LL was more susceptible to compromised mt function after the first hour postmortem. This is evidenced by the clear decline in integrative as well as intrinsic $P_{CI(PM)}$ in LL from 1 h to 24 h, while $P_{CI(PM)}$ in Dia is largely preserved (Figure 3). Curiously, the addition of succinate partially recovered the decline in OXPHOS capacity in LL (Figure 4). To better understand the contribution of CII over time, we calculated P_{CII} (Figure 5A). Integrative P_{CII} was greater in Dia than LL (main effect of muscle: $P < 0.001$) and increased over time in both muscles (main effect of time: $P < 0.001$), with P_{CII} greater at 3 h and 24 h than at 1 h. Intrinsic P_{CII} function tended to increase over time (main effect of time: $P = 0.06$) but was not influenced by muscle (main effect of muscle: $P = 0.87$; muscle × time, $P = 0.46$; Figure 5B). Notably, the increase in P_{CII} postmortem in both muscles suggests that CII may be upregulated in response to declining oxygen concentration, declining pH, or other postmortem stressors. For instance, Lukyanova and Kirova (2015) showed that hypoxia induces reprogramming of respiratory chain function and promotes switching from CI-related substrates to CII substrate (succinate) in the brain, and Pfleger and Abdellatif (2015) demonstrated that activation of CII enhances cell survival during hypoxia. It is also possible that, in the LL, augmented P_{CII} may be compensating for diminished CI activity. This points to compromised function of CI in the LL and/or to steps prior to CI involving substrate transport and enzymatic reactions in the TCA cycle. Similarly, early postmortem factors, such as slow chilling (3–6 h postmortem), were associated with reduced CI activity in permeabilized fibers of bovine *semimembranosus*, and CI-mediated respiration decreased markedly during 3 wk of storage (Phung et al., 2013). Reduced function of CI or TCA enzymes may be due to oxidative damage caused by reactive oxygen species. Several subunits of CI, as well as mt aconitase, are susceptible to oxidative modifications that reduce activity (Yan et al., 1997; Sheeran and Pepe, 2016). Notably, reactive oxygen species metabolism differs between glycolytic and oxidative fibers.

Glycolytic fibers exhibit greater H_2O_2 release, which is largely determined by the balance between superoxide production and H_2O_2 scavenging ability (Anderson and Neufer, 2006). Consistent with this, Picard et al. (2012) showed that glycolytic fibers display lower capacity of antioxidant enzymes, even when adjusted for mt content.

Coupling control factors for complexes I and II

The CCF in the presence of CI substrates (CCF_{CI}) is defined as the fractional change from one respiratory state to another, in this case from leak to $P_{CI(PM)}$ (($P_{CI(PM)} - L$)/$P_{CI(PM)} = 1 - (L/P_{CI(PM)})$; Figure 6A). Accordingly, a greater CCF indicates a greater change from L to P, or greater coupling of oxygen consumption and phosphorylation, and efficiency of the OXPHOS process. We found that time postmortem differentially affected CCF_{CI} in the 2 muscles (muscle × time: $P = 0.03$), with CCF_{CI} in the Dia unchanged over time ($P = 0.87$) but decreasing in the LL ($P < 0.001$). The CCF_{CI+II} (CCF in the presence of CI and CII substrates) was lower in LL compared with Dia (0.93 ± 0.017 in Dia vs. 0.86 ± 0.017 in LL; main effect of muscle: $P < 0.01$; Figure 6B) but was not affected by time postmortem ($P = 0.79$) or an interaction between time and muscle (muscle × time: $P = 0.97$; Figure 6B). The coupling between oxidation and phosphorylation (frequently reported as the respiratory control ratio) is often considered a good indicator of mt quality (Kuznetsov et al., 2008), either giving information about the quality of the mt preparation or about general mt health. The generally greater coupling control in the Dia reflects a more efficient mt respiratory function. While CCF_{CI} declined with time postmortem in the LL, CCF_{CI+II} remained similar over time within muscle, possibly reflecting a compensatory function of CII. Yet we observed clear changes between 1 h and 24 h postmortem in the LL in aspects of mt function (P_{CI}, see earlier) and quality (membrane permeability; cyt c response; see later). Our data suggest that mt in the LL are more affected by postmortem processes than those in the Dia and, furthermore, that CI is more affected than CII, likely contributing more to the overall decline in mt function postmortem.

Cytochrome c response

To test mt outer membrane integrity in the course of time postmortem, exogenous cyt c was added to respiration chambers following P_{CI+II}, before uncoupling with FCCP (see Figure 1). If the outer mt membrane is
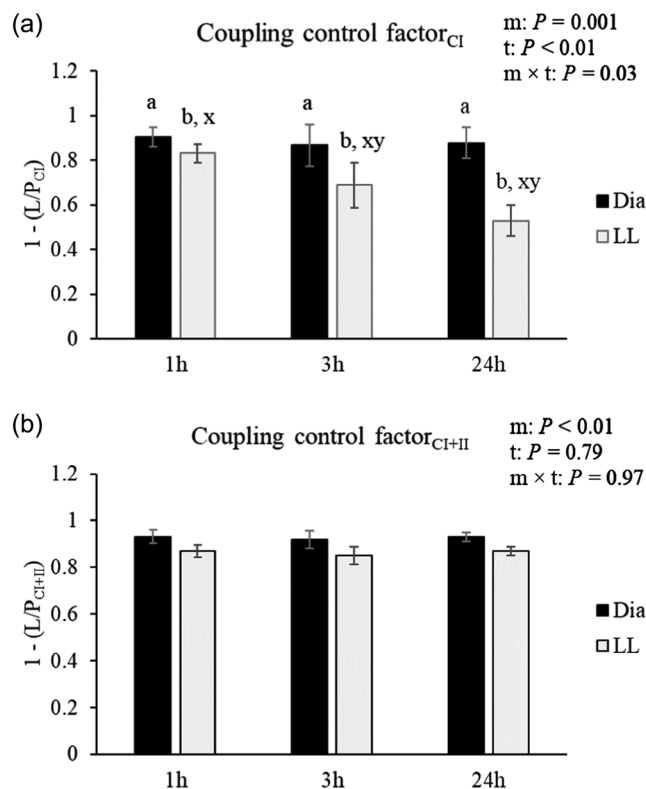
Figure 6. Coupling control factor for (a) CI and (b) CI + CII calculated as $1 - (L/P_{CI})$ and $1 - (L/P_{CI+II})$, respectively, in permeabilized fibers from bovine LL and Dia collected at 1, 3, and 24 h postmortem. [a,b]Different letters represent differences between muscles (muscle effect: $P < 0.05$) within time. [x,y]Different letters represent differences between time point (time effect: $P < 0.05$) within muscle. CI, complex I; CII, complex II; Dia, *diaphragm*; LL, *longissimus lumborum*. m, main effect of muscle; t, main effect of time; m x t, muscle and time interaction.

intact, exogenous cyt c will not enter the mt and OCR should not significantly increase (Kuznetsov et al., 2008). However, an increase in OCR following exogenous cyt c addition indicates outer membrane damage due to sample preparation or naturally induced membrane damage. We found that muscles responded differently during the postmortem period (muscle × time: $P = 0.03$). At 1 h postmortem, the increase in OCR in LL and Dia after cyt c addition was below the previously established threshold (15% increase; Figure 7). Therefore, our teasing and permeabilization protocol was effective and not damaging, and mt outer membrane was preserved at 1 h postmortem. At 3 h postmortem, the mean increase in cyt c response was greater than 15% in both muscles, and the increase in LL tended to be greater than in Dia ($P = 0.06$). At 24 h postmortem, the difference between muscles was significant, with LL exhibiting a greater percentage increase in OCR than Dia (88% vs. 41%; $P = 0.004$). Additionally, within LL, the cyt c response increased considerably from 1 to 3 h ($P < 0.001$) but
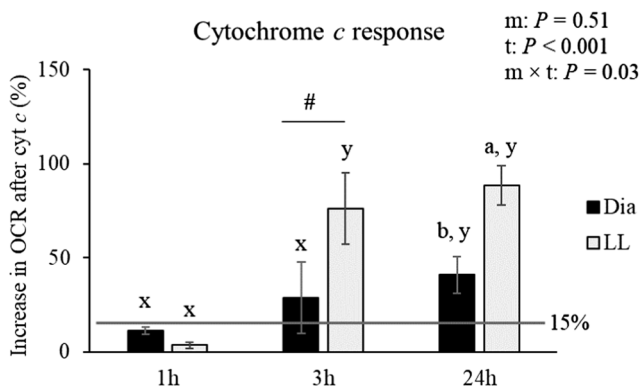
Figure 7. Percentage increase in OCR after addition of exogenous cyt *c* to test mitochondrial outer membrane integrity in permeabilized muscle fibers from bovine LL and Dia collected at 1, 3, and 24 h postmortem. The horizontal line represents previously established threshold (15%). [a,b]Different letters represent differences between muscles (muscle effect: $P < 0.05$) within time. [x,y]Different letters represent differences between time (time effect: $P < 0.05$) within muscle. [#]Represents the trend between muscles within 3 h postmortem ($P = 0.06$). cyt *c*, cytochrome *c*; Dia, *diaphragm*; LL, *longissimus lumborum*; OCR, oxygen consumption rate. m, main effect of muscle; t, main effect of time; m x t, muscle and time interaction.

was similar from 3 to 24 h ($P = 0.16$). In comparison, while the cyt *c* response in the Dia also increased postmortem, it was to a lesser extent than LL and differed only between 1 and 24 h postmortem ($P = 0.02$).

Release of endogenous cyt *c* from the mt into the cytosol is requisite for caspase-mediated cell death and apoptosis. Considering the greater cyt *c* response at 3 h, activation of caspase pathways could be initiated between 1 and 3 h postmortem in bovine LL and Dia. Permeabilization of a small number of mt may be insufficient to trigger apoptosis, particularly in skeletal muscle and other postmitotic cells (Khodjakov et al., 2004; reviewed by Tait and Green, 2010). Several factors may modulate how cells respond to mt outer membrane permeabilization. For example, the proapoptotic protein Apoptotic Protease Activating Factor 1 is expressed at low levels in sympathetic neurons and cardiomyocytes, which are postmitotic cells that have been shown to survive outer mt membrane permeabilization (Potts et al., 2003; Sanchis et al., 2003; Potts et al., 2005). Importantly, apoptosis requires ATP, though the level necessary for caspase activation in postmortem muscle is not clear. However, there are conflicting data regarding caspase involvement in the conversion of muscle to meat (Underwood et al., 2008; Mohrhauser et al., 2011; Cao et al., 2013; Ding et al., 2020; Ramos et al., 2020b), and cyt *c* release does not necessarily mean that apoptosis is occurring, as cyt *c* release may occur prior to necrosis or caspase-independent cell death. Regardless, cell death normally follows mt outer

membrane permeabilization, and our data support that, if caspases contribute to postmortem proteolysis, it is unlikely that they are activated immediately after harvest.

Electron transport system and maximum oxygen consumption rate

Substrates supply electrons for the redox reactions within the mt ETS, which is associated with the relocation of protons from the matrix to the intermembrane space, generating a proton gradient across the inner mt membrane. The resulting proton motive force supports ATP synthesis by the ATP synthase (complex V) during proton flux back to the matrix through complex V. Respiration (oxygen reduction at complex IV) is thereby coupled to the phosphorylation of ADP. Uncoupling agents allow protons to flow back into the mt matrix without passing through complex V, thereby dissipating the electrochemical gradient and the proton motive force, which leads to an uncoupling of respiration (oxygen reduction) from ATP synthesis. In our protocol, titration of the uncoupler FCCP occurred after cyt *c* addition and in the presence of substrates (pyruvate, malate, glutamate, and succinate). At 1 h postmortem, FCCP increased respiration once more, stimulating the ETS to work at maximum capacity without being limited by the phosphorylation system. Overall, FCCP stimulated OCR by 30% in Dia and 20% in LL when compared with P_{CI+II}. However, at 3 h and 24 h postmortem, addition of FCCP sometimes resulted in a decrease in OCR relative to the preceding condition (cyt *c*), indicating that ETS was inhibited rather than stimulated. Adding excessive amounts of uncoupler (FCCP) has an inhibitory effect on OXPHOS because many solute and ion transporters utilize the proton electrochemical potential across the inner mt membrane as a driving force (for review, see Palmieri [2004] and Poburko and Demaurex [2012]), and sensitivity of mt to FCCP can be affected by various conditions and disease states (Demine et al., 2019). Although FCCP was added in a stepwise manner to induce maximal ETS capacity instead of inhibiting it, it is possible that mt in muscle fibers at later times postmortem (3 h and 24 h) were already in a more compromised state and were more sensitive to the effects of FCCP. Therefore, we concluded that, in these cases, using OCR in the presence of FCCP would underestimate ETS capacity. Thus, we elected to use "OCR$_{max}$" to indicate maximal ETS capacity, which we define as a sample's greatest OCR achieved in the presence of either cyt *c* or uncoupler. Integrative
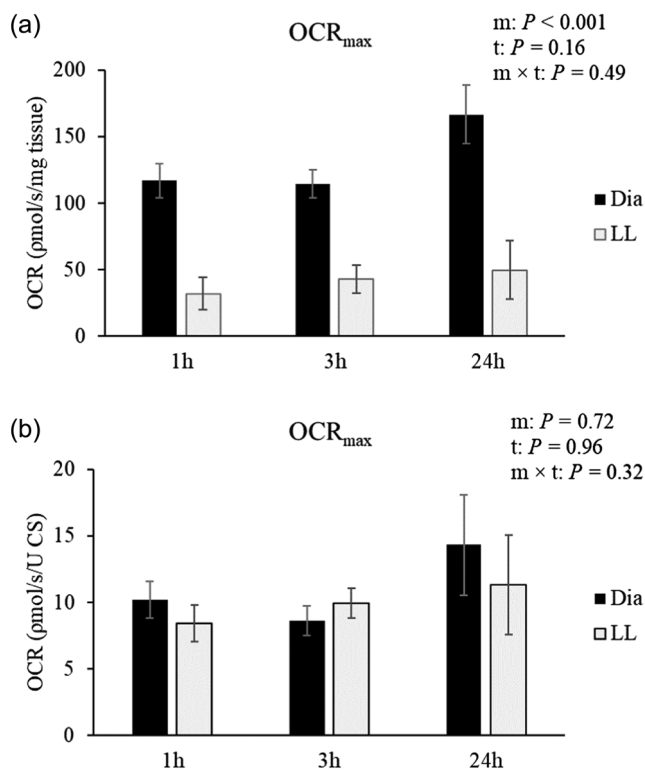
Figure 8. (A) Integrative (ρmol/s/mg wet weight tissue) and (B) intrinsic (ρmol/s/U CS) OCR_{max} representing the greatest rate achieved during the SUIT protocol (corrected for residual oxygen consumption), which occurred either after addition of cyt c or during FCCP titration in permeabilized muscle fibers from bovine LL and Dia collected at 1, 3, and 24 h postmortem. CS, citrate synthase; cyt c, cytochrome c; Dia, *diaphragm*; FCCP, carbonyl cyanide 4-(trifluoromethoxy) phenylhydrazone; LL, *longissimus lumborum*; OCR_{max}, maximum oxygen consumption rate; SUIT, substrate-uncoupler-inhibitor-titration. m, main effect of muscle; t, main effect of time; m x t, muscle and time interaction.

OCR_{max} was dependent on muscle ($P < 0.001$) but not time postmortem ($P = 0.16$) or interaction ($P = 0.49$; Figure 8A). Dia exhibited ~3.7 times greater OCR_{max} than LL, consistent with mt content. In agreement, intrinsic OCR_{max} was not different between muscles ($P = 0.72$) or over time ($P = 0.96$), and there was no interaction between muscle type and time postmortem ($P = 0.32$; Figure 8B).

Excess capacity factor

The ETS excess capacity factor indicates the limitation of OXPHOS by the phosphorylation system (Gnaiger, 2014). A greater excess capacity factor indicates greater "spare" or excess capacity, whereas lower values reflect an OXPHOS system that is operating closer to its maximum ability. In our experiment, OCR_{max} was used to represent ETS capacity, and, similar to CCF, excess capacity factor indicates the fractional change from one respiratory state to another: in this case, P_{CI+II} to OCR_{max} was calculated

as $(OCR_{max} - P_{CI+II})/OCR_{max} = 1 - (P_{CI+II}/OCR_{max})$. Mt excess capacity factor tended to be greater in LL than Dia (main effect of muscle: $P = 0.06$) and differentially affected by time (muscle × time: $P < 0.01$; Figure 9). Spare capacity did not change over time in Dia ($P = 0.51$) but increased postmortem in LL ($P < 0.001$). Spare capacity in the LL increased from 1 to 3 h ($P = 0.008$) and tended to increase from 3 h to 24 h ($P = 0.06$). Our data indicate that the increase in spare capacity in the LL is driven by the numerical decline in P_{CI+II} as well as numerical increase in OCR_{max}, which is related to high cyt c response at 3 h and 24 h postmortem.

The more rapid cyt c response in the LL, along with increasing excess capacity factor, reflect compromised membrane permeability and mt function in glycolytic muscle compared with oxidative muscle. Dutson et al. (1974) used electron microscopy to classify fibers from porcine *longissimus* as red or white (based on mt number and Z-line density) and determined that more extensive mt disruption was associated with the fast fibers at 24 h postmortem. The apparent differences in mt outer membrane integrity between Dia and LL observed here might be linked to calcium homeostasis in the postmortem cellular milieu and to the respective mt calcium storage capacity. Intermyofibrillar mt represent a greater percentage of total mt volume compared with subsarcolemmal mt (Krieger et al., 1980; Hoppeler et al., 1987). In glycolytic fibers, intermyofibrillar mt are small and punctate and organized perpendicular to the axis of contraction (Bleck et al., 2018). Accordingly, mt in glycolytic fibers have greater surface
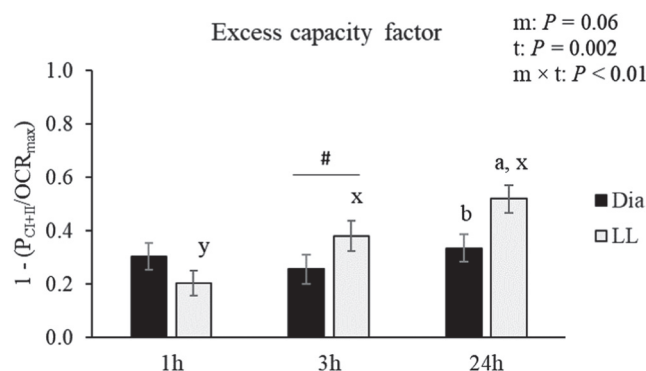
Figure 9. Excess capacity factor calculated as $1 - (P_{CI+II}/OCR_{max})$ in permeabilized fibers from bovine LL and Dia collected at 1, 3, and 24 h postmortem. [a,b]Different letters represent differences between muscles (muscle effect: $P < 0.05$) within time. [x,y]Different letters represent differences between time point (time effect: $P < 0.05$) within muscle. [#]Represents the trend between muscles within 3 h postmortem ($P = 0.07$). Dia, *diaphragm*; LL, *longissimus lumborum*; OCR_{max}, maximum oxygen consumption rate. m, main effect of muscle; t, main effect of time; m x t, muscle and time interaction.

area to volume ratio, facilitating interaction with the cytosolic environment. Mt surface area associated with sarcoplasmic reticulum, another calcium storage site, is also greater in glycolytic muscle, consistent with calcium cycling demands (Bleck et al., 2018). Accordingly, mt from glycolytic fibers are exposed to larger fluctuations in calcium during contractions, which likely contribute to large increases in mt matrix calcium (Picard et al., 2012). When the mt calcium concentration exceeds a certain threshold, mt membrane permeability transition and collapse of the mt membrane potential ensues. Picard et al. (2008) showed that the calcium threshold for permeability transition pore opening was approximately 3 times greater in permeabilized fibers from white *gastrocnemius* than from oxidative *soleus*, indicating that glycolytic muscle may be more resistant to permeability transition and cell death signaling. However, the high cyt *c* response in the LL at 3 h indicates that the calcium concentration may have exceeded the mt threshold in glycolytic fibers and overwhelmed their capacity to resist permeability transition. In contrast, the greater mt content of oxidative fibers may have augmented the total calcium retention capacity, thereby delaying permeability transition. Furthermore, mt in oxidative fibers form elongated networks that are organized in a grid-like manner parallel and perpendicular to myofibrils (Bleck et al., 2018). It is possible that this system is "protecting" mt in Dia, allowing them to redistribute ions or respire longer, whereas the mt from LL may be more exposed and vulnerable to postmortem changes in intracellular ion concentrations. In glycolytic muscle, compromised mt membrane integrity may help hasten activation of proteases by contributing to increase in sarcoplasmic calcium. In turn, this could enhance calpain-mediated proteolysis and tenderization.

Muscle pH and temperature decline

Muscle pH and temperature decline are fundamental factors influencing postmortem metabolism and meat quality development. The LL and Dia exhibited different patterns of temperature decline postmortem (muscle × time: $P < 0.001$; Table 1). Due to its thin shape and minimal fat cover, the Dia was more exposed to environmental temperatures than the LL, which contributed to a more rapid temperature decline. Enzymatic activities are temperature dependent; increasing temperature alone is sufficient to hasten pH decline, accelerate time to rigor, and impact degree of shortening (Marsh, 1954). The Dia and LL also displayed different patterns of pH decline (muscle × time:

Table 1. Temperature and pH decline in bovine *diaphragm* (Dia) and *longissimus lumborum* (LL) collected at 1, 3 and 24h *postmortem*

	Dia	LL	SE
Temp. (°C)			
1 h	38.03[x]	39.18[x]	0.369
3 h	24.08[b,y]	35.17[a,x]	0.998
24 h	3.13[z]	3.95[y]	0.552
pH			
1 h	6.28[b,x]	6.68[a,x]	0.082
3 h	5.89[b,y]	6.15[a,y]	0.049
24 h	5.69[a,z]	5.49[b,z]	0.037
		P-values	
	Muscle (m)	Time (t)	m × t
Temp.	0.021	<0.001	<0.001
pH	0.004	<0.001	<0.001

[1]SE = standard error

[a–b]Different letters represent differences within a row ($P < 0.05$)

[x–z]Different letters represent differences within a column and within response variable ($P < 0.05$)

$P < 0.001$). However, these patterns were inconsistent with the concept of temperature driving pH decline, as Dia had lower pH than the LL at 1 and 3 h postmortem despite a more rapid temperature decline. Importantly, aforementioned results by Marsh (1954) for pH–temperature relationships were obtained by changing temperature of only one muscle (*longissimus*). However, the rate of pH decline early postmortem also depends on muscle fiber properties. Oxidative muscles have been shown to exhibit lower pH early postmortem compared with intermediate/glycolytic muscles; this has been noted in bovine (Koohmaraie et al., 1988; Veiseth-Kent et al., 2018), ovine (Ilian et al., 2001), and pig (Melody et al., 2004). Compared with LL, the lower pH at 1 and 3 h in Dia may also be associated with the lower buffering capacity of oxidative muscles (Lawrie, 1998). Further work is necessary to define the influence of temperature and pH on mt function postmortem in divergent muscle types.

In summary, we showed that mt content was sufficient to explain muscle differences in OXPHOS and ETS capacity between the Dia and LL, and that mt from both muscles retain the ability to produce ATP within 24 h postmortem. However, mt from the 2 muscles exhibited intrinsic differences in leak and coupling control, and those from glycolytic fibers showed earlier mt disruption and loss of functionality, indicated by greater response to cyt *c* and reduced CI activity when compared with oxidative fibers. Due to muscle differences in pH and temperature decline, we cannot exclude the possibility that these parameters contribute to

muscle differences in mt function postmortem. Rapid temperature decline in Dia may help preserve mt function. Phung et al. (2013) showed that bovine *semimembranosus* temperature was negatively associated with OCR. Others have observed that porcine LL with rapid pH decline exhibits a more profound decrease in mt respiratory activity in comparison to LL with slower pH decline (Werner et al., 2010; Popp et al., 2015). Paradoxically, rapid pH decline in Dia does not appear to negatively impact mt function. Thus, the relationship between rate of pH decline and mt function may depend on mt content and mt properties associated with fiber type. Mt in glycolytic fibers appear to be more prone to structural and functional changes postmortem than oxidative fibers, particularly if pH decline is rapid. This may be the result of reduced antioxidant capacity, calcium handling, and limited mechanisms to prevent mt membrane permeability in glycolytic fibers. It is expected, based on presented results, that lower mt content within bovine muscle is associated with faster mt disruption, and earlier reduction in respiration and coupling capacity, which could ultimately affect development of beef quality.

Conclusions

Mt content largely explains differences in OXPHOS and ETS capacity between metabolically distinct muscles, such as the LL and Dia. However, mt in these muscles exhibited divergent responses during the postmortem period, with mt in Dia exhibiting a greater ability to retain functionality and integrity despite a more rapid pH decline. Specialized properties associated with fiber type, including antioxidant capacity, calcium handling, and resistance to outer membrane permeability transition, may contribute to different patterns between muscle fiber types postmortem. In conjunction, these intrinsic mt properties modulate oxidative damage and protease activity, which are important parameters affecting the conversion of muscle to meat.

Acknowledgments

Literature Cited

Adhihetty, P. J., V. Ljubicic, K. J. Menzies, and D. A. Hood. 2005. Differential susceptibility of subsarcolemmal and intermyofibrillar mitochondria to apoptotic stimuli. Am. J. Physiol.-Cell Ph. 289:C944–C1001. https://doi.org/10.1152/ajpcell.00031.2005.

Anderson, E. J., and P. D. Neufer. 2006. Type II skeletal myofibers possess unique properties that potentiate mitochondrial H_2O_2 generation. Am. J. Physiol.-Cell Ph. 290:844–851. https://doi.org/10.1152/ajpcell.00402.2005.

Ashmore, C. R., W. Parker, and L. Doerr. 1972. Respiration of mitochondria isolated from dark-cutting beef: postmortem changes. J. Anim. Sci. 34:46–48.

Bleck, C. K. E., Y. Kim, T. B. Willingham, and B. Glancy. 2018. Subcellular connectomic analyses of energy networks in striated muscle. Nat. Commun. 9:1–11. https://doi.org/10.1038/s41467-018-07676-y.

Bock, F. J., and S. W. G. Tait. 2020. Mitochondria as multifaceted regulators of cell death. Nat. Rev. Mol. Cell. Bio. 21:85–100. https://doi.org/10.1038/s41580-019-0173-8.

Boncompagni, S., A. E. Rossi, M. Micaroni, G. V. Beznoussenko, R. S. Polishuk, R. T. Dirksen, and F. Protasi. 2009. Mitochondria are linked to calcium stores in striated muscle by developmentally regulated tethering structures. Mol. Biol. Cell. 20:1058–1067. https://doi.org/10.1091/mbc.e08-07-0783.

Brand, M. D. 2000. Uncoupling to survive? The role of mitochondrial inefficiency in ageing. Exp. Gerontol. 35:811–820. https://doi.org/10.1016/s0531-5565(00)00135-2.

Cao, J. X., C. R. Ou, Y. F. Zou, K. P. Ye, Q. Q. Zhang, M. A. Khan, D. D. Pan, and G. Zhou. 2013. Activation of caspase-3 and its correlation with shear force in bovine skeletal muscles during postmortem conditioning. J. Anim. Sci. 91:4547–4552. https://doi.org/10.2527/jas2013-6469.

Demine, S., P. Renard, and T. Arnould. 2019. Mitochondrial uncoupling: A key controller of biological processes in physiology and diseases. Cells. 8:795. https://doi.org/10.3390/cells8080795.

Ding, Z., Q. Wei, C. Zhang, H. Zhang, and F. Huang. 2020. Influence of oxidation on Heat Shock Protein 27 translocation, caspase-3 and calpain activities and myofibrils degradation in postmortem beef muscles. Food Chem. 340:127914. https://doi.org/10.1016/j.foodchem.2020.127914.

Dutson, T. R., A. M. Pearson, R. A. Merkel, and G. C. Spink. 1974. Ultrastructural postmortem changes in normal and low quality porcine muscle fibers. J. Food Sci. 39:32–37.

Eigentler, A., M. Fontana-Ayoub, M. Fasching, B. Lassnig, S. Stadlmann, G. Rieger, B. Haffner, H. Lemieux, and E. Gnaiger. 2012. Selected media and chemicals for respirometry with mitochondria and permeabilized cells. Mitochondrial Physiol. Netw. 03.02:1–9.

England, E. M., S. K. Matarneh, R. M. Mitacek, A. Abraham, R. Ramanathan, J. C. Wicks, H. Shi, T. L. Scheffler, E. M. Oliver, E. T. Helm, and D. E. Gerrard. 2018. Presence of oxygen and mitochondria in skeletal muscle early postmortem. Meat Sci. 139:97–106. https://doi.org/10.1016/j.meatsci.2017.12.008.

Fasching, M., M. Fontana-Ayoub, and E. Gnaiger. 2016. Oroboros O2k-protocols chemicals: Mitochondrial respiration medium-MiR06, version 06. Mitochondrial Physiol. Netw. 14.13:1–4.

Glancy, B., and R. S. Balaban. 2011. Protein composition and function of red and white skeletal muscle mitochondria. Am. J. Physiol.-Cell Ph. 300:C1280–C1290. https://doi.org/10.1152/ajpcell.00496.2010.

Gnaiger, E. 2014. Mitochondrial pathways and respiratory control. An introduction to OXPHOS analysis. 4th ed. Mitochondrial Physiol. Netw. 19.12. Oroboros MiPNet Publications, Innsbruck: 80 pp.

Halestrap, A. P. 2009. What is the mitochondrial permeability transition pore? J. Mol. Cell. Cardiol. 46:821–831. https://doi.org/10.1016/j.yjmcc.2009.02.021.

Hofer, T., S. Servais, A. Y. Seo, E. Marzetti, A. Hiona, S. J. Upadhyay, S. E. Wohlgemuth, and C. Leeuwenburgh. 2009. Bioenergetics and permeability transition pore opening in heart subsarcolemmal and interfibrillar mitochondria: Effects of aging and lifelong calorie restriction. Mech. Ageing Dev. 130:297–307. https://doi.org/10.1016/j.mad.2009.01.004.

Hoppeler, B. Y. H., O. Hudlicka, and E. Uhlmann. 1987. Relationship between mitochondria and oxygen consumption in isolated cat muscles. J. Physiol.-London. 385:661–675. https://doi.org/10.1113/jphysiol.1987.sp016513.

Ilian, M. A., J. D. Morton, M. P. Kent, C. E. Le Couteur, J. Hickford, R. Cowley, and R. Bickerstaffe. 2001. Intermuscular variation in tenderness: Association with the ubiquitous and muscle-specific calpains. J. Anim. Sci. 79:122–132. https://doi.org/10.2527/2001.791122x.

Karch, J., and J. D. Molkentin. 2015. Review– Regulated necrotic cell death: the passive aggressive side of Bax and Bak. Circ. Res. 1800–1809. https://doi.org/10.1161/CIRCRESAHA.116.305421.

Khodjakov, A., C. Rieder, C. A. Mannella, and K. W. Kinnally. 2004. Laser micro-irradiation of mitochondria: is there an amplified mitochondrial death signal in neural cells? Mitochondrion. 3:217–227. https://doi.org/10.1016/j.mito.2003.10.002.

Koohmaraie, M., S. C. Seideman, J. E. Schollmeyer, T. R. Dutson, and A. S. Babiker. 1988. Factors associated with the tenderness of three bovine muscles. J. Food Sci. 53:407–410. https://doi.org/10.1111/j.1365-2621.1988.tb07717.x.

Korzeniewski, B. 2017. Contribution of proton leak to oxygen consumption in skeletal muscle during intense exercise is very low despite large contribution at rest. PLoS One. 12:1–14. https://doi.org/10.1371/journal.pone.0185991.

Krieger, D. A., C. A. Tate, J. McMillin-Wood, and F. W. Booth. 1980. Populations of rat skeletal muscle mitochondria after exercise and immobilization. J. Appl. Physiol. 48:23–28. https://doi.org/10.1152/jappl.1980.48.1.23.

Kuznetsov, A. V., V. Veksler, F. N. Gellerich, V. Saks, R. Margreiter, and W. S. Kunz. 2008. Analysis of mitochondrial function in situ in permeabilized muscle fibers, tissues and cells. Nat. Protoc. 3:965–976. https://doi.org/10.1038/nprot.2008.61.

Kwong, J. Q., and J. D. Molkentin. 2015. Physiological and pathological roles of the mitochondrial permeability transition pore in the heart. Cell Metab. 21:206–214. https://doi.org/10.1016/j.cmet.2014.12.001.

Larsen, S., J. Nielsen, C. N. Hansen, L. B. Nielsen, F. Wibrand, N. Stride, H. D. Schroder, R. Boushel, J. W. Helge, F. Dela, and M. Hey-Mogensen. 2012. Biomarkers of mitochondrial content in skeletal muscle of healthy young human subjects. J. Physiol.-London. 590:3349–3360. https://doi.org/10.1113/jphysiol.2012.230185.

Lawrie, R. A., editor. 1998. Lawrie's Meat Science. 6th ed. Woodhead Publishing, Cambridge.

Leary, S. C., C. N. Lyons, A. G. Rosenberger, J. S. Ballantyne, J. Stillman, and C. D. Moyes. 2003. Fiber-type differences in muscle mitochondrial profiles. Am. J. Physiol.-Reg. I. 285: R817–R826. https://doi.org/10.1152/ajpregu.00058.2003.

Li, C., S. H. White, L. K. Warren, and S. E. Wohlgemuth. 2016. Effects of aging on mitochondrial function in skeletal muscle of American American Quarter Horses. J. Appl. Physiol. 121:299–311. https://doi.org/10.1152/japplphysiol.01077.2015.

Liu, X., C. N. Kim, J. Yang, R. Jemmerson, and X. Wang. 1996. Induction of apoptotic program in cell-free extracts: Requirement for dATP and cytochrome c. Cell. 86:147–157. https://doi.org/10.1016/S0092-8674(00)80085-9.

Lukyanova, L. D., and Y. I. Kirova 2015. Mitochondria-controlled signaling mechanisms of brain protection in hypoxia. Front. Neurosci.-Switz. 9:320. https://doi.org/10.3389/fnins.2015.00320.

Marsh, B. B. 1954. Effects of early post-mortem pH and temperature on beef tenderness. J. Sci. Food Agr. 5:70–75. https://doi.org/10.1002/jsfa.2740050202.

Melody, J. L., S. M. Lonergan, L. J. Rowe, T. W. Huiatt, M. S. Mayes, and E. Huff-Lonergan. 2004. Early postmortem biochemical factors influence tenderness and water-holding capacity of three porcine muscles. J. Anim. Sci. 82:1195–1205. https://doi.org/10.1016/j.meatsci.2005.05.014.

Mohrhauser, D. A., K. R. Underwood, and A. D. Weaver. 2011. In vitro degradation of bovine myofibrils is caused by μ-calpain, not caspase-3. J. Anim. Sci. 89:798–808. https://doi.org/10.2527/jas.2010-3149.

Muroya, S., I. Nakajima, and K. Chikuni. 2002. Related expression of MyoD and Myf5 with myosin heavy chain isoform types in bovine adult skeletal muscles. Zool. Sci. 19:755–761. https://doi.org/10.2108/zsj.19.755.

Palmer, J. W., B. Tandler, and C. L. Hoppel. 1977. Biochemical properties of subsarcolemmal and interfibrillar mitochondria isolated from rat cardiac muscle. J. Biol. Chem. 252:8731–8739.

Palmieri, F. 2004. The mitochondrial transporter family (SLC25): Physiological and pathological implications. Pflug. Arch. Eur. J. Phy. 447:689–709. https://doi.org/10.1007/s00424-003-1099-7.

Park, S., J. R. Gifford, R. H. I. Andtbacka, J. D. Trinity, J. R. Hyngstrom, R. S. Garten, N. A. Diakos, S. J. Ives, F. Dela, S. Larsen, S. Drakos, and R. S. Richardson. 2014. Cardiac, skeletal, and smooth muscle mitochondrial respiration: are all mitochondria created equal? Am. J. Physiol.-Heart C. 307:346–352. https://doi.org/10.1152/ajpheart.00227.2014.

Pfleger, J., and M. Abdellatif. 2015. Mitochondrial complex II is a source of the reserve respiratory capacity that is regulated by metabolic sensors and promotes cell survival. Cell Death Dis. 6:e1835. https://doi.org/10.1038/cddis.2015.202.

Phung, V. T., M. Khatri, K. H. Liland, E. Slinde, O. Sørheim, T. Almøy, K. Saarem, and B. Egelandsdal. 2013. Mitochondrial oxygen consumption in permeabilized fibers and its link to colour changes in bovine M. semimembranosus muscle. Meat Sci. 93:128–137. https://doi.org/10.1016/j.meatsci.2012.08.016.

Picard, M., K. Csukly, M. E. Robillard, R. Godin, A. Ascah, C. Bourcier-Lucas, and Y. Burelle. 2008. Resistance to Ca2+-induced opening of the permeability transition pore differs in mitochondria from glycolytic and oxidative muscles. Am. J. Physiol.-Reg. I. 295:659–668. https://doi.org/10.1152/ajpregu.90357.2008.

Picard, M., R. T. Hepple, and Y. Burelle. 2012. Mitochondrial functional specialization in glycolytic and oxidative muscle fibers: tailoring the organelle for optimal function. Am. J. Physiol.-Cell Ph. 302:C629–C641. https://doi.org/10.1152/ajpcell.00368.2011.

Picard, M., D. Ritchie, K. J. Wright, C. Romestaing, M. M. Thomas, S. L. Rowan, T. Taivassalo, and R. T. Hepple. 2010. Mitochondrial functional impairment with aging is exaggerated in isolated mitochondria compared to permeabilized myofibers. Aging Cell. 9:1032–1046. https://doi.org/10.1111/j.1474-9726.2010.00628.x.

Poburko, D., and N. Demaurex. 2012. Regulation of the mitochondrial proton gradient by cytosolic Ca2+ signals. Plug. Arch. Eur. J. Phy. 464:19–26. https://doi.org/10.1007/s00424-012-1106-y.

Popp, J., M. Wicke, G. Klein, and C. Krischek. 2015. The relationship of pork longissimus muscle pH to mitochondrial respiratory activities, meat quality and muscle structure. Animal. 9:356–361. https://doi.org/10.1017/S1751731114002365.

Potts, P. R., S. Singh, M. Knezek, C. B. Thompson, and M. Deshmukh. 2003. Critical function of endogenous XIAP in regulating caspase activation during sympathetic neuronal apoptosis. J. Cell Biol. 163:789–799. https://doi.org/10.1083/jcb.200307130.

Potts, M. B., A. E. Vaughn, H. McDonough, C. Patterson, and M. Deshmukh. 2005. Reduced Apaf-1 levels in cardiomyocytes engage strict regulation of apoptosis by endogenous XIAP. J. Cell Biol. 171:925–930. https://doi.org/10.1083/jcb.200504082.

Powers, S. K., L. L. Ji, A. N. Kavazis, and M. J. Jackson. 2011. Reactive oxygen species: Impact on skeletal muscle. Compr. Physiol. 1:941–969. https://doi.org/10.1002/cphy.c100054.

Ramos, P. M., C. Li, M. A. Elzo, S. E. Wohlgemuth, and T. L. Scheffler. 2020a. Mitochondrial oxygen consumption in early postmortem permeabilized skeletal muscle fibers is influenced by cattle breed. J. Anim. Sci. 98. https://doi.org/10.1093/jas/skaa044.

Ramos, P. M., S. A. Wright, E. F. Delgado, E. Van Santen, D. D. Johnson, J. M. Scheffler, M. A. Elzo, C. C. Carr, and T. L. Scheffler. 2020b. Resistance to pH decline and slower calpain-1 autolysis are associated with higher energy availability early postmortem in Bos taurus indicus cattle.

Meat Sci. 159:107925. https://doi.org/10.1016/j.meatsci.2019.107925.

Sanchis, D., M. Mayorga, M. Ballester, and J. X. Comella. 2003. Lack of Apaf-1 expression confers resistance to cytochrome c-driven apoptosis in cardiomyocytes. Cell Death Differ. 10:977–986. https://doi.org/10.1038/sj.cdd.4401267.

Scheffler, T. L., M. B. Leitner, and S. A. Wright. 2018. Technical note: Protocol for electrophoretic separation of bovine myosin heavy chain isoforms and comparison to immunohistochemistry analysis 1. J. Anim. Sci. 4306–4312. https://doi.org/10.1093/jas/sky283.

Schmidt, I., and P. Herpin. 1998. Carnitine palmitoyltransferase I (CPT I) activity and its regulation by malonyl-CoA are modulated by age and cold exposure in skeletal muscle mitochondria from newborn pigs. J. Nutr. 128:886–893. https://doi.org/10.1093/jn/128.5.886.

Sheeran, F. L., and S. Pepe. 2016. Posttranslational modifications and dysfunction of mitochondrial enzymes in human heart failure. Am. J. Physiol.-Endoc. M. 311:449–460. https://doi.org/10.1152/ajpendo.00127.2016.

Skulachev, V. P. 1996. Role of uncoupled and non-coupled oxidations in maintenance of safely low levels of oxygen and its one-electron reductants. Q. Rev. Biophys. 29:169–202. https://doi.org/10.1017/S0033583500005795.

Sollanek, K. J., J. G. Burniston, A. N. Kavazis, A. B. Morton, M. P. Wiggs, B. Ahn, A. J. Smuder, and S. K. Powers. 2017. Global proteome changes in the rat diaphragm induced by endurance exercise training. PLoS ONE. 12:e0171007. https://doi.org/10.1371/journal.pone.0171007.

Tait, S. W. G., and D. R. Green. 2010. Mitochondria and cell death: outer membrane permeabilization and beyond. Nat. Rev. Mol. Cell Bio. 11:621–632. https://doi.org/10.1038/nrm2952.

Tang, J., C. Faustman, T. A. Hoagland, R. A. Mancini, M. Seyfert, and M. C. Hunt. 2005. Postmortem oxygen consumption by mitochondria and its effects on myoglobin form and stability. J. Agr. Food Chem. 53:1223–1230. https://doi.org/10.1021/jf048646o.

Toniolo, L., L. Maccatrozzo, M. Patruno, F. Caliaro, F. Mascarello, and C. Reggiani. 2005. Expression of eight distinct MHC isoforms in bovine striated muscles: Evidence for MHC-2B presence only in extraocular muscles. J. Exp. Biol. 208: 4243–4253. https://doi.org/10.1242/jeb.01904.

Underwood, K. R., W. J. Means, and M. Du. 2008. Caspase 3 is not likely involved in the postmortem tenderization of beef muscle. J. Anim. Sci. 86:960–966. https://doi.org/10.2527/jas.2007-0549.

Varikmaa, M., R. Bagur, T. Kaambre, A. Grichine, N. Timohhina, K. Tepp, I. Shevchuk, V. Chekulayev, M. Metsis, F. Boucher, V. Saks, A. V. Kuznetsov, and R. Guzun. 2014. Role of mitochondria-cytoskeleton interactions in respiration regulation and mitochondrial organization in striated muscles. BBA-Bioenergetics. 1837:232–245. https://doi.org/10.1016/j.bbabio.2013.10.011.

Veiseth-Kent, E., M. E. Pedersen, S. B. Rønning, and R. Rødbotten. 2018. Can postmortem proteolysis explain tenderness differences in various bovine muscles? Meat Sci. 137:114–122. https://doi.org/10.1016/j.meatsci.2017.11.011.

Wadley, G. D., and G. K. McConell. 2007. Effect of nitric oxide synthase inhibition on water absorption in rat jejunum. J. Appl. Physiol. 102:314–320. https://doi.org/10.1152/japplphysiol.00549.2006.

Werner, C., R. Natter, K. Schellander, and M. Wicke. 2010. Mitochondrial respiratory activity in porcine longissimus muscle fibers of different pig genetics in relation to their meat quality. Meat Sci. 85:127–133. https://doi.org/10.1016/j.meatsci.2009.12.016.

Williams, G. S. B., L. Boyman, A. C. Chikando, R. J. Khairallah, and W. J. Lederer. 2013. Mitochondrial calcium uptake. P. Natl. Acad. Sci. USA. 110:10479–10486. https://doi.org/10.1073/pnas.1300410110/-/DCSupplemental.

Wright, S. A., P. Ramos, D. D. Johnson, J. M. Scheffler, M. A. Elzo, R. G. Mateescu, A. L. Bass, C. C. Carr, and T. L. Scheffler. 2018. Brahman genetics influence muscle fiber properties, protein degradation, and tenderness in an Angus-Brahman multibreed herd. Meat Sci. 135:84–93. https://doi.org/10.1016/j.meatsci.2017.09.006.

Yan, L.-J., R. L. Levine, and R. S. Sohal. 1997. Oxidative damage during aging targets mitochondrial aconitase. P. Natl. Acad. Sci. USA. 94:11168–11172. https://doi.org/10.1073/pnas.94.21.11168.